

# Supplementary materials for

## Nonlinear Thermal Emission and Visible Thermometry

Zhihao Zhou<sup>1</sup>, Wei Liu<sup>2</sup>, Hengzhe Yan<sup>1</sup>, Xianfeng Chen<sup>2</sup>, and Wenjie Wan<sup>1,2\*</sup>

<sup>1</sup>The State Key Laboratory of Advanced Optical Communication Systems and Networks,

University of Michigan-Shanghai Jiao Tong University Joint Institute,

Shanghai Jiao Tong University, Shanghai 200240, China

<sup>2</sup>Department of Physics and Astronomy, Shanghai Jiao Tong University, Shanghai 200240, China

\*Corresponding author: Wenjie Wan [wenjie.wan@sjtu.edu.cn](mailto:wenjie.wan@sjtu.edu.cn)

### S1. Estimation of the thermal upconversion efficiency

A theoretical value of the thermal radiation upconversion efficiency can be estimated by starting with the expression of SFG efficiency below, which is derived from Eq. (2) in manuscript.

$$\eta(\lambda_{\text{vis}}) = \frac{I_{\text{vis}}}{I_{\text{IR}}} = \frac{8\pi^2}{\epsilon_0 c \lambda_{\text{vis}}^2} \frac{N \langle |d_{\text{eff}}|^2 \rangle}{n_{\text{vis}} n_{\text{pump}} n_{\text{IR}}} \langle X^2 \text{sinc}^2(\Delta k X / 2) \rangle I_{\text{pump}}$$

From the above expression, the only disparity between different wavelength pairs' conversion efficiency is caused by the factor  $1/(\lambda_{\text{vis}}^{-2} \times n_{\text{vis}} \times n_{\text{IR}})$ . To roughly estimate, we can start with an arbitrary wavelength pair as an example, say,  $\lambda_{\text{vis}} = 800\text{nm}$ ,  $\lambda_{\text{IR}} = 1/(1/\lambda_{\text{vis}} - 1/\lambda_{\text{pump}}) = 3.22\mu\text{m}$ . And the average effective nonlinear coefficient can be considered as  $\langle |d_{\text{eff}}|^2 \rangle = \text{mean}(d_{33}^2, d_{31}^2, d_{22}^2)$  of LiNbO<sub>3</sub> by incorporating all the orientations[37], which gives a value about  $488(\text{pm}/V)^2$ . What need to be treated carefully is the averaged phase mismatch factor

$$\langle X^2 \text{sinc}^2(\Delta k X / 2) \rangle = \int_0^\infty X^2 \text{sinc}^2(\Delta k X / 2) p(X) dX$$

which can be evaluated by substituting the specific probability distribution of propagation length

$p(X) = \frac{1}{\sqrt{2\pi}\sigma} e^{-(X-\mu)/2\sigma^2}$  into the expression. To use an accurate number for our case, statistical data from our used nanocrystal need to be figured out, which can be obtained by processing and analyzing the sample's SEM images.

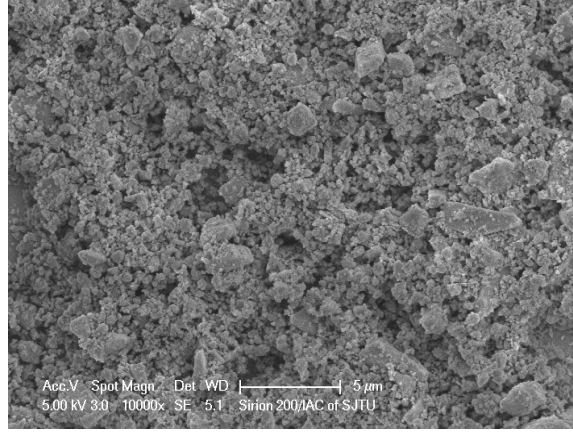


**Fig. S1** Overview of nanocrystal thin film sample

An example of a specific ROI is shown below, first, the SEM image is enhanced to better show the miniaturized nanocrystals. The enhanced image is then binarized and followed with several steps of image filtering. With post processing as well as image analyzing, we then get the statistical distribution from the captured SEM image [Fig. S2(b)],

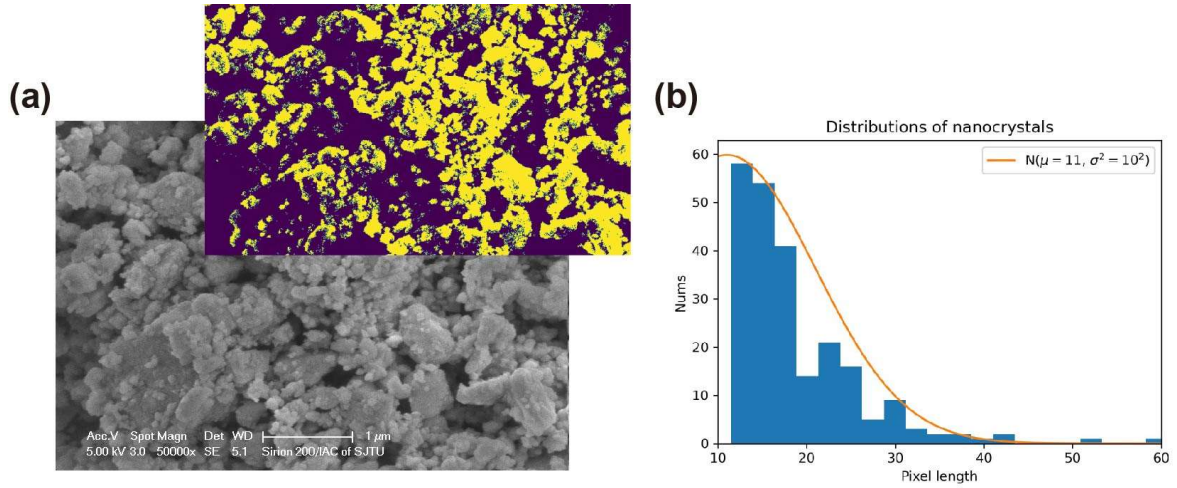


**Fig. S2** (a) SEM and binarized image of an ROI (b) Statistical distribution obtained from processing

where a single pixel is estimated to be  $\sim 8\text{nm}$  in length. With all these above constants determined, the SFG efficiency of 800nm signal can then be calculated and further simplified, which now becomes  $\eta = 2.1 \times 10^{-12} \mu\text{m}^2 / W \times I_{\text{pump}} \times N$ .

In our current work, the pump laser intensity is about  $I_{\text{pump}} = 0.5W / (\pi * (150\mu\text{m})^2)$ , and  $N \approx 2 \times \text{film\_thickness} / \text{domain\_length} \approx 1100$ . Hence the number of efficiency is estimated to be  $\eta = 1.7 \times 10^{-14}$ . As we can see, the overall efficiency scales linearly with  $I_{\text{pump}} \times N$ , which means we can increase either the pump intensity or nanocrystal thickness to promote the nonlinear conversion efficiency.

Another factor that dramatically affects the efficiency is the size of nanocrystals when compared with coherence length of nonlinear interactions  $L_{\text{coh}} = 2 / \Delta k$ . In this work, the number of coherence length is about  $3.5\mu\text{m}$  because of the presence of mid-IR waves. However, current sizes of nanocrystals are restricted to be less than  $300\text{nm}$  as shown in Fig. S2(b), which halts the overall efficiency. Further improvements of conversion efficiency can be achieved if domain length as well as film thickness are optimized according to the interacting wavelengths.

## S2. Signal-Temperature calibration curve

Fig. 5(b) in manuscript is fitted with  $\sum \ln^{\text{Signal}(\lambda_{\text{vis}}, T)} \propto T^{-1}$ . To get the relationship, we can start from Eq. (3) in manuscript, that

$$I_{\text{vis}}(\lambda_{\text{vis}}, \lambda_{\text{IR}}, T) \propto \frac{1}{\lambda_{\text{vis}}^2} I_{\text{IR}}(\lambda_{\text{IR}}, T) = \frac{1}{\lambda_{\text{vis}}^2} \varepsilon(\lambda_{\text{IR}}) B(\lambda_{\text{IR}}, T) = \frac{1}{\lambda_{\text{vis}}^2} \alpha(\lambda_{\text{IR}}) B(\lambda_{\text{IR}}, T)$$

First, by taking logarithm to base  $e$  on both sides, we can get

$$\ln I_{\text{vis}}(\lambda_{\text{vis}}, \lambda_{\text{IR}}, T) = C_1 + \ln \frac{1}{\lambda_{\text{vis}}^2} + \ln \alpha(\lambda_{\text{IR}}) + \ln B(\lambda_{\text{IR}}, T)$$

then substituting the expression of Planck distribution into the equation, the explicit form of right-hand side regarding  $T$  can be derived to be

$$\ln I_{\text{vis}}(\lambda_{\text{vis}}, \lambda_{\text{IR}}, T) = C_1 + \ln \frac{1}{\lambda_{\text{vis}}^2} + \ln \alpha(\lambda_{\text{IR}}) + \ln 2hc^2 / \lambda_{\text{IR}}^5 - \ln e^{hc / (\lambda_{\text{IR}} k_B T) - 1}$$

Because  $e^{hc / (\lambda_{\text{IR}} k_B T)} \gg 1$  always holds for  $\lambda_{\text{IR}} T \sim 1200 \mu\text{m} \cdot \text{K}$ , which is roughly our experimental conditions. The equation can be further simplified, and now it becomes

$$\ln I_{\text{vis}}(\lambda_{\text{vis}}, \lambda_{\text{IR}}, T) = C_1 + \ln \frac{1}{\lambda_{\text{vis}}^2} + \ln \alpha(\lambda_{\text{IR}}) + \ln 2hc^2 / \lambda_{\text{IR}}^5 - \frac{hc}{\lambda_{\text{IR}} k_B T}$$

This temperature dependence of signal holds for all the wavelength pairs  $(\lambda_{\text{vis}}, \lambda_{\text{IR}})$ . Thus, for any specific visible wavelength range, the below relation is always satisfied,

$$\sum_{\lambda_{\text{vis}}} \ln^{\text{Signal}(\lambda_{\text{vis}}, T)} = \sum_{\lambda_{\text{vis}}} C_1 + C_2 - \sum_{\lambda_{\text{IR}}} \frac{hc}{\lambda_{\text{IR}} k_B} \times \frac{1}{T}$$

where  $C_2 = \sum_{\lambda_{\text{vis}}} (\ln \frac{1}{\lambda_{\text{vis}}^2} + \ln \alpha(\lambda_{\text{IR}}) + \ln 2hc^2 / \lambda_{\text{IR}}^5)$  and  $\lambda_{\text{vis}} = 1 / (1/1064 + 1/\lambda_{\text{IR}})$ . Hence, an inverse proportional relationship  $\sum \ln^{\text{Signal}(\lambda_{\text{vis}}, T)} \propto T^{-1}$  between signal and temperature is expected.

### S3. Comparative experiment to exclude potential sources of signal

In our experiment, there are several steps we take to prepare the nanocrystal film sample, which can be listed as:

1. Grind  $\text{LiNbO}_3$  into nanocrystals with an alumina ceramic mortar (99%  $\text{Al}_2\text{O}_3$ )
2. Supersonically dissolve  $\text{LiNbO}_3$  nanocrystal powder along with a very little  $\text{Mg}(\text{NO}_3)_2 \cdot 6\text{H}_2\text{O}$  into isopropanol, here  $\text{Mg}(\text{NO}_3)_2 \cdot 6\text{H}_2\text{O}$  is used to help move nanocrystals towards the cathode
3. Insert metal electrode pads as well as ITO glass into the solution and apply voltage on both sides
4. Wait some time and finally a thin film of  $\text{LiNbO}_3$  nanocrystals will form on top of ITO substrate

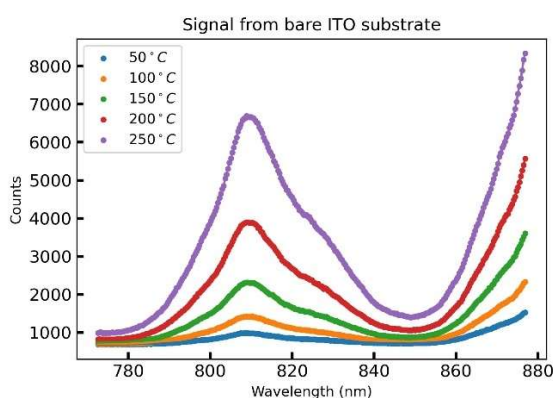
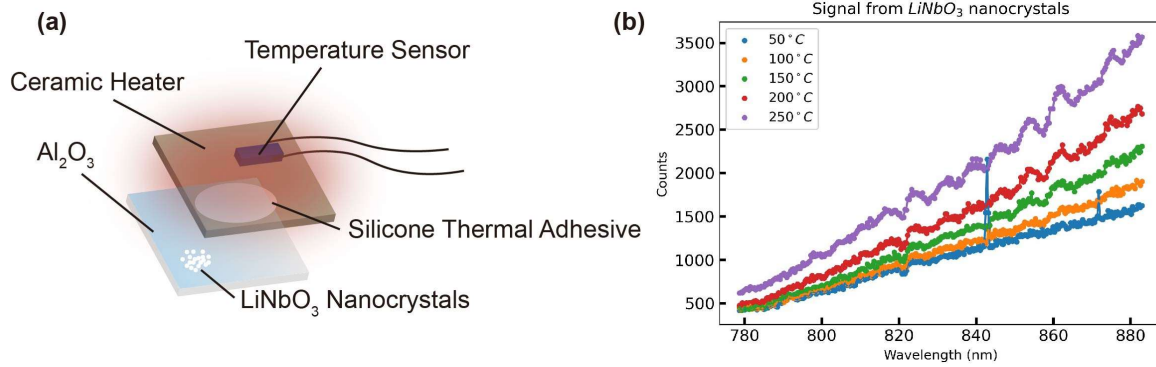


Fig. S3 Signal from a bare ITO substrate under different temperature with 250mW pump laser

First, in order to check whether the collected signal is from ITO glass substrate, we experimentally verify the spectrum of bare ITO substrate with the same heating strategy as well as 1064nm laser pumping. The measured signal from bare ITO glass is plotted in Fig. S3, where the profiles are quite different from the measured spectral signal in our manuscript. To further exclude all the other potential factors during sample preparation that may affect our conclusion as well as the influence of ITO glass, we also do a comparative experiment of sample preparation by removing steps 2 - 4 listed above.

As an alternative, we dissolve the  $\text{LiNbO}_3$  nanocrystals into deionized water. And then we drip the solution onto a  $\text{Al}_2\text{O}_3$  substrate instead, and place it on a heater to evaporate the water. We also place the  $\text{Al}_2\text{O}_3$  substrate with an offset on the ceramic heater to totally isolate the  $\text{LiNbO}_3$  nanocrystal sample from those lower side materials but with only  $\text{Al}_2\text{O}_3$  substrate beneath like Fig. S4(a) shows. In this way, we are able to collect a much cleaner signal.



**Fig. S4** (a) Schematic of the comparative experiment and (b) Collected spectral signal under varying temperature and 170mW pump laser

Results in Fig. S4(b) shows that quite similar temperature-dependent signals as Fig. 3 in our manuscript can still be observed, and no signals are ever detected on bare Al<sub>2</sub>O<sub>3</sub> nearby, which gives us confidence that the observed signal is from LiNbO<sub>3</sub> itself. Note that in the comparative experiment, because temperature sensor is placed on the heater, the setting temperature might not accurately represent that of nanocrystal aggregates. For Al<sub>2</sub>O<sub>3</sub> crystalline, we can know from other related researches that its spectrum is quite clear under an intense pulsed laser, like Fig. S5 below shows[39]. In their work, they pumped the sapphire wafer with an intense femto-second laser at 1.595 $\mu$ m. As their results shows, the collected signal at 750 – 850nm wavelength range is quite clear no matter under which crystalline orientation, and only the THG signal is observed, which help us exclude the possibility that the signal is originated from Al<sub>2</sub>O<sub>3</sub> substrate.

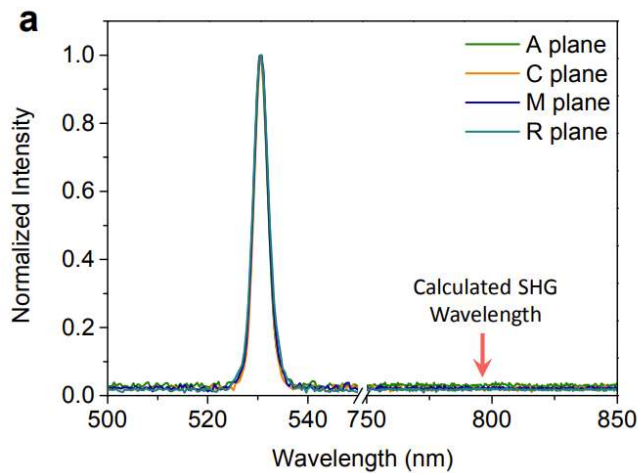


**Fig. S5** THG spectra from A, C, M and R-plane sapphire wafers pumped with femto-second laser at 1.595 $\mu$ m[39]